

# DFT study of water adsorption on lignite molecule surface

Zhengyang Gao<sup>1</sup> · Yi Ding<sup>1</sup> · Weijie Yang<sup>1</sup> · Wentao Han<sup>1</sup>

Received: 2 November 2016 / Accepted: 15 December 2016  
© Springer-Verlag Berlin Heidelberg 2017

**Abstract** High moisture content is a main characteristic of low-rank coal, such as lignite. Numerous oxygen containing functional groups in lignite make it represent some special properties, and these functional groups affect the adsorption mechanisms of water molecules on lignite surface. This study reports some typical water ··· lignite conformations, along with a detailed analysis of the geometry, electrostatic potential distribution, reduced density gradient of interaction, and interaction energy decomposition. The results show that water molecules tend to aggregate around functional groups, and hydrogen bonds play a dominant role in the interaction. The adsorption energy of water cluster on lignite surface is larger than that of isolated water molecule, a good linear relationship between the interaction distance and adsorption energy of layers has been found. Since water is a polar molecule, the local minima and maxima of electrostatic potential in conformations increase along with more water adsorbing on lignite surface. Reduced density gradient analysis shows that H-bonds, van der Waals interaction, and a little steric make up the interaction between water cluster and lignite molecule. In these studied conformations which mainly are H-bond complexes, electrostatic and exchange repulsion play a dominant role, whereas polarization and dispersion make relatively small contribution to the interaction. Attractive and repulsive interaction both affect the stability of water ··· lignite conformations.

**Keywords** Electrostatic potential · Energy decomposition analysis · Lignite · Reduced density gradient · Water adsorption

## Introduction

Coals play an important role in supplying primary energy in the world [1], but the coal deposit around the globe will last about 150 years at the current rate of use [2]. Low-rank coals have huge reserves and distribute widely in the world [3], and low-rank lignite has been burned in numerous coal-fired plants in China. Lignite generally features high volatile and moisture content and low ignition temperature. And lignite has high oxygen content (15~30%) in oxygen containing functional groups compared with that of high-rank coals [4]. The order of functional group content from high to low is: phenolic hydroxyl, alcohol hydroxyl, carbonyl, and methoxyl. High oxygen content and substantial pores in lignite lead to easy spontaneous combustion.

Water in lignite coal has significant influence on its utilization processes, such as desiccation, pyrolysis, and combustion. On the one hand, high moisture content in lignite results in low boiler efficiency compared with other high-rank coal-burned boiler; on the other hand, massive heat from combustion of lignite is wasted in removing the water [5], which makes combustion unstable at low running load [6, 7]. The forms of water in lignite influence the ease of water removal, during water removing, the changes in structure of lignite are significant and this can impact the coal reactivity in downstream applications [8].

With the deeper extent of coalification, the water content in coal decreases correspondingly. High-rank coal with low water content is most probably due to elimination of polar functional groups especially oxygen containing functional groups

✉ Weijie Yang  
18331121421@163.com

<sup>1</sup> The Department of Power Engineering, North China Electric Power University, Baoding 071003, China

[9, 10]. Suuberg et al. [11, 12] suggested that lignite exhibits a gel-like behavior, and swells and shrinks obviously correspond to the loss and gain of water. The oxygen containing functional groups like carboxyl and hydroxyl groups play an important role in adsorbing water, as these groups are removed, the lignite gradually loses its hydrophilicity [13].

The form of water in coals depends on many factors like intermolecular hydrogen bonding [14–16], intermolecular van der Waals interaction, and water clusters [17, 18]. Three main types of water-coal bonds exist: adsorbed water by physicochemical forces, free water held by physicochemical forces, and chemically bonded water [19, 20]. Coal surface functional groups contain only oxygen like carbonyl adsorb water via H bond acceptor, while hydroxyl and carboxyl groups containing both oxygen and hydrogen can act either as H bond donors and acceptors [21]. Kaij and Švábová [18, 22] demonstrated that there exist a good correlation between these hydrophilic sites and the water adsorption capacity of coal. Nishino [23] suggested that acidic carboxyl groups are the predominant site of adsorption compared with other oxygen containing functional groups. The monolayer waters are attached to the coal mostly by hydrogen bonding at oxygen containing functional groups [21], and the monolayer waters can provide adsorption sites for secondary waters and then water clusters are formed around functional groups [24]. The high oxygen content of coal means that more oxygen containing functional groups in coal, and numerous adsorption sites can easily adsorb water molecules to form water clusters [25].

Kumagai et al. [26] established the  $C_{21}H_{20}O_7$  pentamer model to simulate the interaction between Yalloum coal and water based on the data of elemental analysis and nuclear magnetic resonance (NMR) spectroscopy. They simulated the moisture removal process, initially, 360 water molecules were generated to surround the coal model molecule, the initial energy and volume of the minimum energy conformation were recorded. Then, Kumagai calculated the energy and volume of configuration in the process of removing water molecules. Finally, they concluded that removal of water molecules results in a plastic deformation for coal model. Vu et al. [27] utilized lignin to simulate lignite molecule, they built three lignin-water molecular systems (including three lignin monomers and 470 water molecules) for the modeling studies. The results indicated that a hydrogen bond has formed between water and lignin molecules, and therefore, the diffusion of water molecules in the lignin-water systems was significantly weak.

An understanding of water adsorption and binding behavior in the lignite is important to the development of more efficient drying technologies. However, most of the related literature researched the interaction between water and coal molecules based on a relatively small complex system, just selected a local segment of coal and a little water molecules to simulate coal ··· water complex and did not study the

adsorption of water cluster on coal surface. Also, the data about how molecular electrostatic distribution affects the water adsorption and detailed interaction energy components of coal ··· water complexes are still deficient. This paper sought the adsorption mechanisms of water and lignite molecules, together with the visualization of interaction between water and lignite molecules.

## Computational details

### General computational details

All geometries involved in this study were optimized by BLYP density functional method [28] in combination with Grimme's DFT-D3 dispersion correction using Becke-Johnson damping function [29] and Grimme's gCP for BSSE correction [30], and basis set def2-TZVP [31] was adopted. BLYP-D3 is an ideal method for studying large systems because it can successfully research the interaction between large systems, meanwhile, it can save computing time and resources. And this method has proven many times in the past that it provides satisfactory results for non-covalent interactions [32–36]. Single point energy of all optimized configurations was evaluated by double-hybrid functional PWPB95 [37] with DFT-D3 (BJ), and basis set def2-QZVPP(-g, -f) [31] was employed. The accuracy of PWPB95-D3 (BJ)/def2-QZVPP level is close to the accepted golden standard CCSD(T)/CBS [38, 39]. Zero-point correction energies of all configurations were obtained by harmonic frequency calculation at BLYP-D3-gCP/def2-TZVP based on the geometry optimized at the same level. All geometries optimization calculations, single point and zero-point correction energies calculations were realized by ORCA 3.0.1 [40], and in order to save the computational time, resolution-of-identity (RI) technique [41] was used for accelerating self-consistent field (SCF). The error of accuracy due to RI is negligible [39].

LMO-EDA energy decomposition analysis [42] was realized by GAMESS-US program [43], the interaction energy between two monomers can be decomposed to electrostatic energy, exchange energy, repulsion energy, polarization energy, and DFT dispersion energy. Due to a large amount of atoms in the studied configurations, considering the computation time and hardware of ours, GGA functional BLYP and basis set 6-31+G(d,p) were employed. Dispersion effect can not be researched by BLYP density functional method, but this problem can be accurately resolved via combining with Grimme's DFT-D3 dispersion correction [30]. BLYP-D3/6-31+G(d,p) level was used to get dispersion correction energy via ORCA 3.0.1 program. Because the BLYP/6-31+G(d,p) level was not accurate to compute interaction energy, the calculation results of LMO-EDA energy decomposition can only be used for qualitative analysis.

Molecular electrostatic potential on van der Waals surface and reduced density gradient [44] of water ··· lignite configurations were computed by Multiwfn program [45]. All isosurface maps of configurations were plotted by VMD 1.9.1 program [46]. Followed by Lu [38], the grid spacings were set to 0.2 Bohr in the calculation of electrostatic potential. The van der Waals surface referred throughout this paper denotes the isosurface of  $\rho = 0.001e/\text{bohr}^3$  according to Bader [47].

### Lignite modeling specificities

According to the lignite coal model proposed by Kumagai [26], the unit structure was constructed on the basis of element analysis and  $^{13}\text{C}$ -NMR spectroscopy of the coal. Kumagai had demonstrated that this model can represent the characteristics of lignite coal in the moisture release progress. In this paper, hydrogen atom and methyl group were used to complete vacant sites of lignite model unit structure, as shown in Fig. 1. There are hydroxyl, carboxyl, carbonyl, methoxyl, two benzene rings, and one pentabasic cycle in this lignite coal model, and the mass fraction of hydrogen, carbon, oxygen are 6.0%, 66.0%, and 28.0%, respectively. There is no obvious symmetry in this lignite model.

### Water cluster modeling

The open form of dimer, the cyclic forms of trimer and tetramer have been considered the most stable configuration of simple water polymers [48]. Saha et al. [49] proposed a dimer-based two-body interaction model for the study of water clusters using a fragmentation approach, this model accurately reproduces the total energies of water cluster ranging in size from 16 to 100 molecules. Li et al. [50] presented a generalized energy-based fragmentation (GEBF) approach for

approximately predicting the ground-state energies and molecular properties of large molecules, especially for polar molecules. This approach can provide satisfactory ground-state energies, the dipole moments, and static polarizabilities for polar molecules such as water clusters. Dahlke et al. [51] presented electrostatically embedded two-body and three-body expansions for calculating the energies of molecular clusters, this method divides the system into several fragments and it does not use an iterative method to determine the charges and thus provides substantial savings for large clusters. Yuan et al. [52] systematically evaluated the performance of the generalized energy based fragmentation (GEBF) method and the electrostatically embedded many-body (EE-MB) method for medium-size water clusters  $(\text{H}_2\text{O})_n$  ( $n = 10, 20, 30$ ). In this paper, we build rectangular water clusters via combining with water dimer, trimer and tetramer, and the main forms include  $(\text{H}_2\text{O})_6$  cluster in binding with dimer and tetramer,  $(\text{H}_2\text{O})_7$  cluster in binding with trimer and tetramer, and  $(\text{H}_2\text{O})_n$  clusters with  $n = 10, 11$ , and 12. And the calculation of binding energy of water clusters was realized by EE-MB method [51, 52], in this method, a molecular cluster is divided into fragments and its ground-state is expressed as a many-body expansion as follows:

$$E_{total} = \sum_{i=1}^N E_i + \sum_{i=1}^N \sum_{i<j}^N \Delta E_{ij} + \sum_{i=1}^N \sum_{i<j}^N \sum_{j<k}^N \Delta E_{ijk} + \dots \quad (1)$$

$E_i$  ( $E_{ij}$ ) are the energies of fragments (or fragment pairs),  $\Delta E_{ij}$  is the interaction between fragments  $i$  and  $j$ ,  $E_{ijk}$  is the interaction of three-body  $i, j$ , and  $k$ .

$$\Delta E_{ij} = E_{ij} - (E_i + E_j) \quad (2)$$

$$\Delta E_{ijk} = E_{ijk} - (\Delta E_{ij} + \Delta E_{ik} + \Delta E_{jk}) - (E_i + E_j + E_k) \quad (3)$$

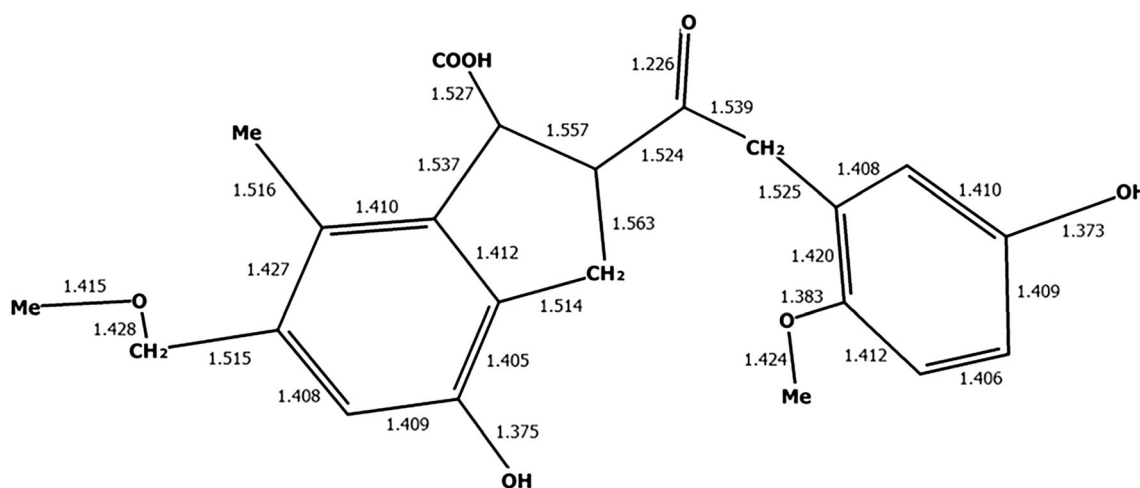


**Fig. 1** Unit structure of lignite molecule. Me represents  $-\text{CH}_3$  group

## Results and discussion

### Adsorption of monolayer water molecule

An isolated water molecule was placed on the lignite surface to simulate the adsorption of single water on lignite surface, single water adsorbed on the oxygen containing functional groups, and formed stable adsorption configurations are shown in Fig. 2, and corresponding interaction energies are shown in Table 1.

It is shown in Fig. 2 that single water adsorbs on lignite surface mainly via interaction between H atoms and O atoms with the H-O distance from 1.78 to 2.29 Å. The calculated adsorption energies are from  $-2.25$  to  $-6.68$  kcal mol $^{-1}$ , which indicate that the interaction between single water and lignite is weak and attributes to physical adsorption. The H-bond energy for water with surface groups should be about 10–14 kJ mol $^{-1}$ , which is consistent with the mechanism of the physical adsorption process [53]. The largest interaction energy is  $-6.68$  kcal mol $^{-1}$  of single water adsorbs on carboxyl group, for which Wu et al. [54] calculated the interaction energy of benzoic acid  $\cdots$  water is  $-51$  kJ mol $^{-1}$ . In Fig. 2b, there exists a strong hydrogen bond between H atom in carboxyl and O atom in water, moreover, the other H atom in water is attracted by the other O atom in carboxyl via electrostatic attraction. The single water molecule combines with carboxyl group to form a ring, and the hydrogen bond is shorter than that of other configurations, thus the structure is more stable and adsorption energy is large for  $-COOH \cdots 1st-H_2O$  configuration. In

literature [21], strong hydrogen bonds have been observed between H<sub>2</sub>O and carboxylic groups, structural studies have revealed very short  $-C(=O)-O-H \cdots OH_2$  bonds ( $<2.5$  Å). In contrast, the value of interaction energy for  $(-OH + -C=O) \cdots 1st-H_2O$  configuration is  $-2.25$  kcal mol $^{-1}$  which is minimal, which indicates that this interaction is physical adsorption.

As shown in Fig. 3, the more stable adsorption geometry of water dimer or water trimer that combines with hydroxyl group is circle structure. The  $-OH \cdots 1st-(H_2O)_2$  configuration can be formed via two ways, the first way is water dimer adsorbs on hydroxyl group and the interaction energy is  $-8.77$  kcal mol $^{-1}$ ; the second way is single water adsorbs on  $-OH \cdots 1st-H_2O$  configuration and the interaction energy is  $-7.13$  kcal mol $^{-1}$ . Also, the  $-COOH \cdots 1st-(H_2O)_2$ ,  $(-COOH + R-O-R) \cdots 1st-(H_2O)_2$  and  $(-OH + -C=O) \cdots 1st-(H_2O)_2$  configurations can be built by the two ways mentioned above, and corresponding adsorption energies are listed in Table 2. The first row in Table 2 contains interaction energy values of water dimer adsorbs on the functional group and the other rows contain interaction energy values of secondary water adsorbs on the functional group which has already adsorbed one water molecule. Secondary water adsorbs on the first adsorbed water and oxygen containing functional group via two H-bonds, which is just like the water dimer through to cyclic trimer. In Table 2, the interaction energies of secondary water adsorbed on the first adsorbed water and functional group are  $-4.88$ ,  $-7.13$ ,  $-10.83$ , and  $-14.24$  kcal mol $^{-1}$ , and the mean changed energy of water dimer through to cyclic trimer is  $-10.75$  kcal mol $^{-1}$

**Fig. 2** Optimized structures of the adsorption of single water on (a) hydroxyl group, (b) carboxyl group, (c) carboxyl and ether, (d) hydroxyl and carbonyl group. The yellow, red, and blue ball represent carbon, oxygen, and hydrogen atom, respectively. The H-O distances are also marked

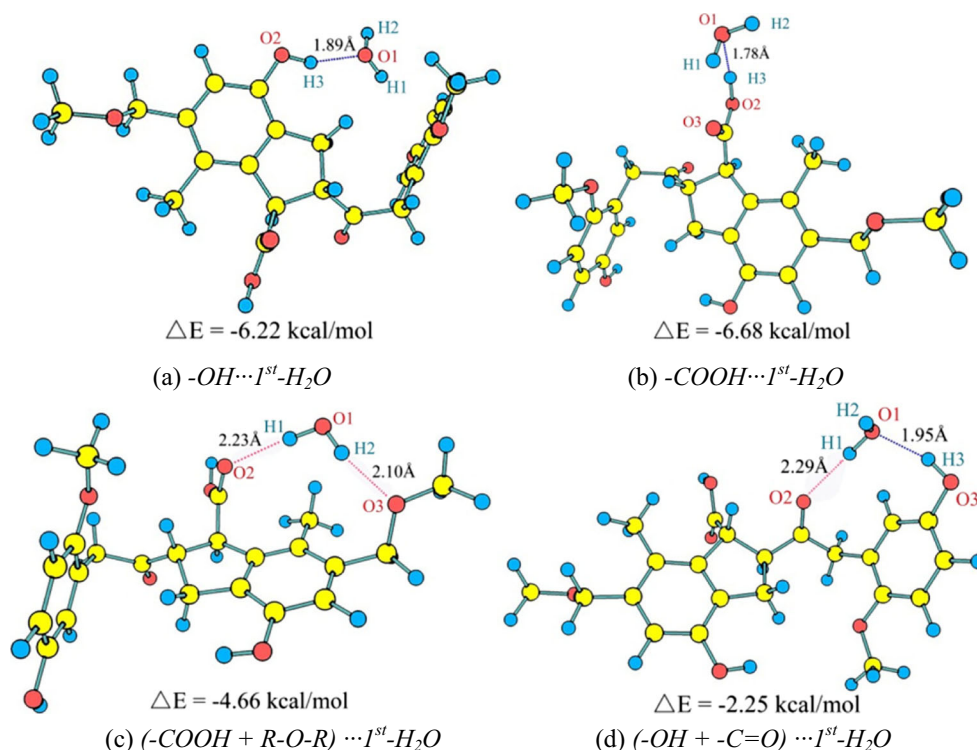


**Table 1** Interaction energy of single water adsorbs on lignite surface

Configurations	$E_{SP}$ (a.u.)	$E_{ZPE}$ (a.u.)	$E_{total}$ (a.u.)	$E_{ads}$ (kcal mol <sup>-1</sup> )
H <sub>2</sub> O	-76.4567	0.0212	-76.4355	0
Lignite	-1379.6602	0.4118	-1379.2484	
$-OH \cdots 1st-H_2O$	-1456.1298	0.4360	-1455.6938	-6.22
$-COOH \cdots 1st-H_2O$	-1456.1327	0.4382	-1455.6945	-6.68
$(-COOH + R-O-R) \cdots 1st-H_2O$	-1456.1304	0.4391	-1455.6913	-4.66
$(-OH + -C=O) \cdots 1st-H_2O$	-1456.1268	0.4393	-1455.6875	-2.25

$E_{SP}$  is single-point energy;  $E_{ZPE}$  is zero-point correction energy;  $E_{total}$  is the sum of  $E_{SP}$  and  $E_{ZPE}$ ;  $E_{ads}$  is adsorption energy

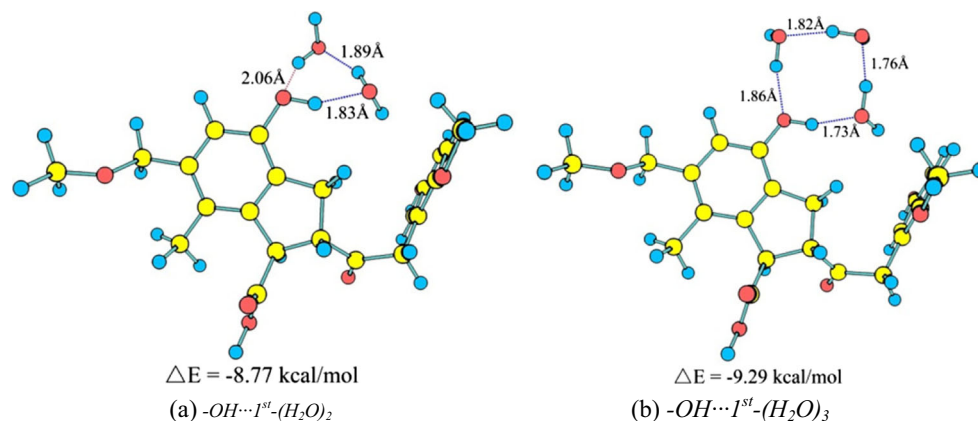
(from -6.10 to -16.84 kcal mol<sup>-1</sup>) which obtained by Del Bene and Pope [55]. Similarly, as shown in Fig. 4a and b, water dimer and water trimer are easier to adsorb on carboxyl group in ring structure. There exist two configurations for water tetramer adsorbs on carboxyl group in the vertical and horizontal direction, respectively, as shown in Fig. 4c and d, and corresponding interaction energies are -8.45 kcal mol<sup>-1</sup> and -12.69 kcal mol<sup>-1</sup>. It indicates that water tetramer is more stable to adsorb horizontally on carboxyl because three hydrogen bonds have been formed between water tetramer and functional groups.

Comparing with the interaction energy of single water and water dimer adsorb on different oxygen containing functional group, it can be found that absolute value of the former is smaller than the latter, which indicates that water dimer is easier to adsorb on oxygen containing functional groups than single water. As shown in Table 1 and Table 2, the interaction energy of single water adsorbs on hydroxyl group is -6.22 kcal mol<sup>-1</sup>, whereas the interaction energy of secondary free water adsorbs on the same hydroxyl group in  $-OH \cdots 1st-H_2O$  configuration is -7.13 kcal mol<sup>-1</sup> in other configurations. These results indicate that oxygen containing functional group which had adsorbed a single water is more active to adsorb other water molecules, and that means the first adsorbed water can provide adsorption sites for other free water and can promote the adsorption of more water molecules.

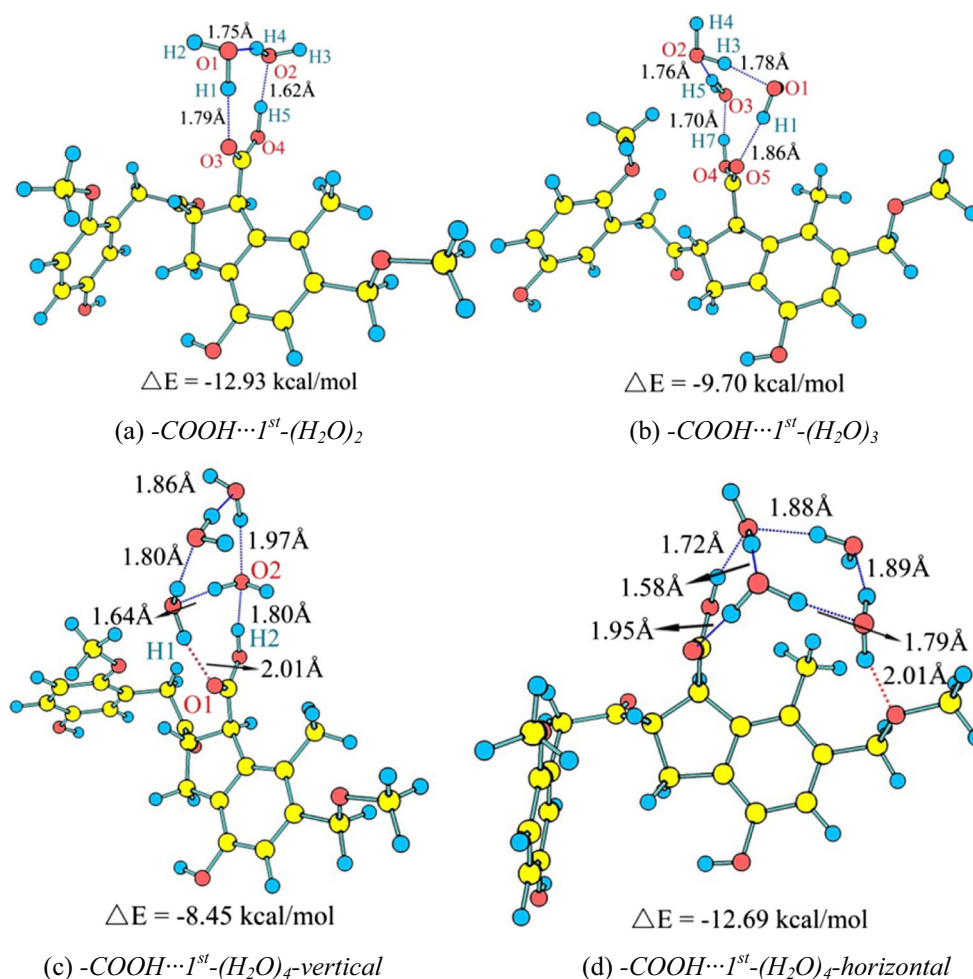
As shown in Table 2, the interaction energy of water dimer that adsorbs on the carboxyl functional group is the largest comparing with other adsorption

configurations. It indicates that water dimer is easier to adsorb on carboxyl, the reasons are carboxyl can provide hydrogen atom as H bond acceptor and oxygen atom as H bond donor, and carboxyl combines with water dimer to form a stable ring. In contrast, the adsorption energy of the  $(-COOH + R-O-R) \cdots 1st-(H_2O)_2$  configuration which water dimer adsorbs on carboxyl and ether group is minimal. As shown in Fig. 5a, the H bond distances between water dimer and oxygen containing functional group are longer than that of  $(-OH + -C=O) \cdots 1st-(H_2O)_2$  configuration. Therefore, the strength of hydrogen bond is relatively weak in  $(-COOH + R-O-R) \cdots 1st-(H_2O)_2$  configuration, and this water  $\cdots$  lignite complex is not stable.

As shown in Table 3, it can be found that the adsorption energy of  $(-OH + -C=O) \cdots 1st-(H_2O)_3$  configuration is the largest compared with other configurations. In Fig. 6b, it is found that water trimer stably adsorbs both on carbonyl and two hydroxyl groups via forming three hydrogen bonds. Similarly, water trimer can adsorb on carboxyl group and form a ring structure in  $-COOH \cdots 1st-(H_2O)_3$  configuration, and the mean length of H-O bonds is as short as 1.78 Å, water molecules can attract each other closely. In contrast, the interaction energy of  $(-COOH + R-O-R) \cdots 1st-(H_2O)_3$  configuration is weak, there exist only two hydrogen bonds between water trimer and lignite, and in addition the H-O bond lengths are relatively long. Therefore, the  $(-COOH + R-O-R) \cdots 1st-(H_2O)_3$  complex is not stable.

**Fig. 3** Optimized structures of the adsorption of (a) water dimer and (b) water trimer on hydroxyl group

**Fig. 4** Optimized structures of the adsorption of (a) water dimer on carboxyl group, (b) water trimer on carboxyl group, water tetramer on carboxyl group in (c) vertical and (d) horizontal



Comparing with the configurations of  $-COOH \cdots 1^{st}-(H_2O)_4$ -vertical,  $(-COOH + R-O-R) \cdots 1^{st}-(H_2O)_4$ , and  $(-OH + -C=O) \cdots 1^{st}-(H_2O)_4$ , it is found that water tetramer adsorbs on lignite surface via two hydrogen bonds, and the adsorption energies are similar to each other. Whereas the adsorption energy of  $-COOH \cdots 1^{st}-(H_2O)_4$ -horizontal configuration is the largest. Stated thus, it is shown that the more hydrogen bonds formed between water clusters and lignite surface, the more stable for adsorption geometries.

For configurations and corresponding interaction energies like  $-COOH \cdots 1^{st}-(H_2O)_4$ -horizontal ( $-12.69$  kcal mol $^{-1}$ ),  $(-COOH + R-O-R) \cdots 1^{st}-(H_2O)_4$  ( $-8.67$  kcal mol $^{-1}$ ),  $(-OH + -C=O) \cdots 1^{st}-(H_2O)_3$  ( $-12.25$  kcal mol $^{-1}$ ), and  $(-OH + -C=O) \cdots 1^{st}-(H_2O)_4$  ( $-8.12$  kcal mol $^{-1}$ ), water trimer or tetramer covers the partial lignite surface. McCutcheon et al. [24] suggested that the net heat of adsorption of water monolayer on coal surface varies from 12 to 16 kJ mol $^{-1}$  (corresponding to water monolayers of coverage ranges from 0.25 to 0.12), which convert to adsorption energy 8.61 to

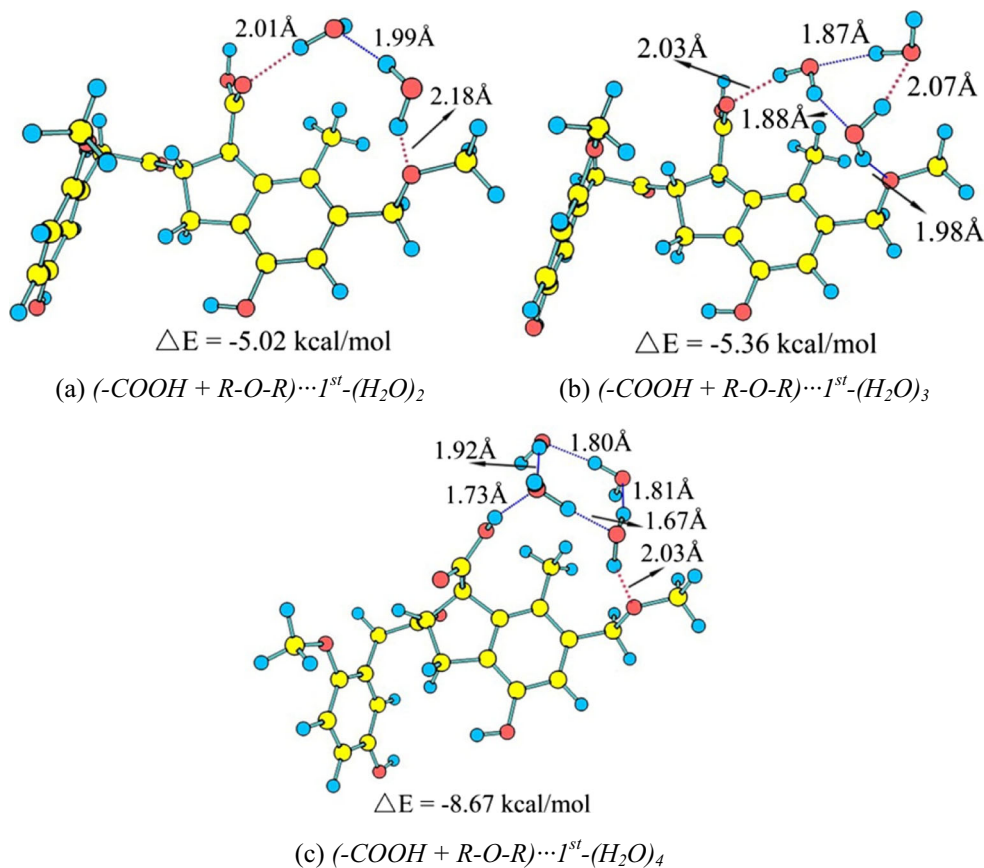
**Table 2** Interaction energy of water dimer/single adsorbs on lignite surface<sup>a</sup>

Configurations	$-OH \cdots 1^{st}-(H_2O)_2$	$-COOH \cdots 1^{st}-(H_2O)_2$	$(-COOH + R-O-R) \cdots 1^{st}-(H_2O)_2$	$(-OH + -C=O) \cdots 1^{st}-(H_2O)_2$
Lignite + (H <sub>2</sub> O) <sub>2</sub>	-8.77	-12.93	-5.02	-11.92
$-OH \cdots 1^{st}-(H_2O) + H_2O$	-7.13	-	-	-
$-COOH \cdots 1^{st}-(H_2O) + H_2O$	-	-10.83	-	-
$(-COOH + R-O-R) \cdots 1^{st}-(H_2O) + H_2O$	-	-	-4.88	-
$(-OH + -C=O) \cdots 1^{st}-(H_2O) + H_2O$	-	-	-	-14.24

The values in table are obtained via energy of the first column configurations subtracted from other columns configurations

<sup>a</sup> Energy is in kcal mol $^{-1}$

**Fig. 5** Optimized structures of the adsorption of (a) water dimer, (b) water trimer, and (c) water tetramer on carboxyl and ether group



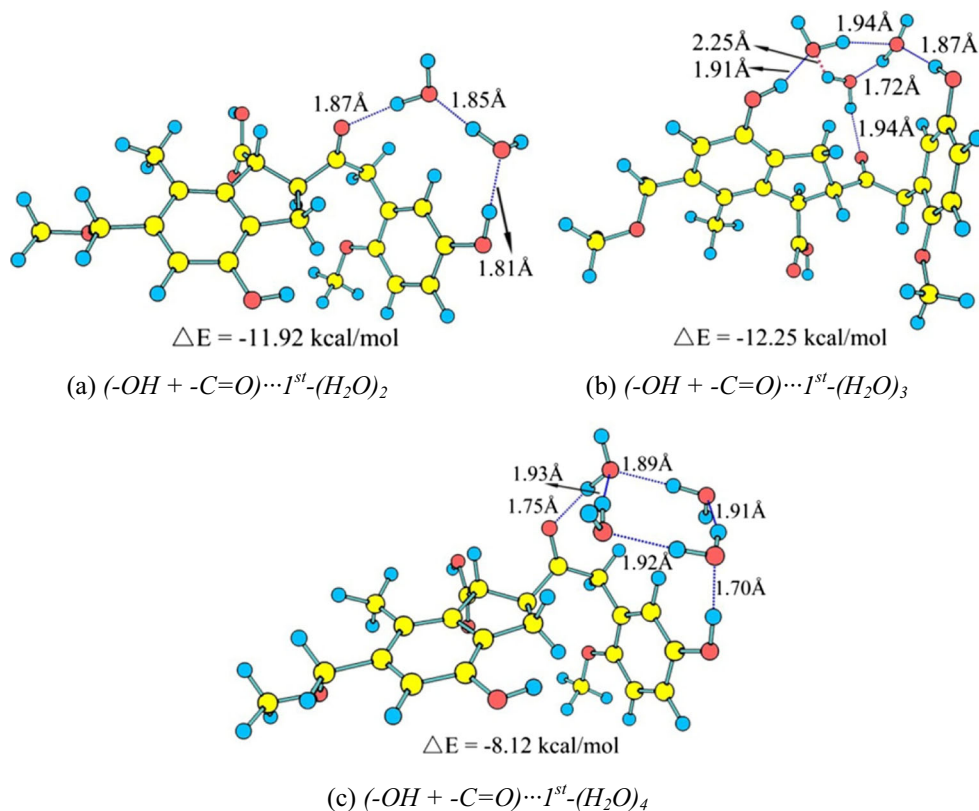
9.80 kcal mol<sup>-1</sup>. Since, the net heat is the difference between the isosteric heat and the latent heat, and the isosteric should be similar to molecular adsorption. Qi et al. [15] presented that heat released during water adsorption is close to the heat of condensation, which is approximately 45 kJ mol<sup>-1</sup>. Salame et al. [56] presented that the heats of water adsorption ( $Q_{st}$ ) have similar shapes with the plateau at the value of  $Q_{st}$  close to 45 kJ mol<sup>-1</sup> with coverage rate of water monolayer on coal up to 0.6. When coverage rate of water monolayer is close to zero, the heats of water adsorption are approximately 17 kJ

mol<sup>-1</sup>, and experimental error is about  $\pm 5$  kJ mol<sup>-1</sup> at low surface coverage. Similarly, values calculated from carefully measured isotherms by Naono et al. [57] on hydrophobic microporous activated carbons and the heat showed an increasing trend with adsorption coverage, from 15 to 32 kJ mol<sup>-1</sup>. The author suggested that the trend was due to an increase of energy from more water-water interactions. An increase in the heat of adsorption is considered due to increasing contributions of H-bond between functional groups and other water molecules [53].

**Table 3** Interaction energy of water trimer/tetramer adsorbs on lignite surface

Configurations	$E_{SP}$ (a.u.)	$E_{ZPE}$ (a.u.)	$E_{total}$ (a.u.)	$E_{ads}$ (kcal mol <sup>-1</sup> )
Lignite + (H <sub>2</sub> O) <sub>3</sub>	-1609.0568	0.4794	-1608.5774	0
-OH ··· 1st-(H <sub>2</sub> O) <sub>3</sub>	-1609.0777	0.4854	-1608.5922	-9.29
-COOH ··· 1st-(H <sub>2</sub> O) <sub>3</sub>	-1609.0793	0.4865	-1608.5928	-9.70
(-COOH + R-O-R) ··· 1st-(H <sub>2</sub> O) <sub>3</sub>	-1609.0734	0.4875	-1608.5859	-5.36
(-OH + -C = O) ··· 1st-(H <sub>2</sub> O) <sub>3</sub>	-1609.0830	0.4861	-1608.5969	-12.25
Lignite + (H <sub>2</sub> O) <sub>4</sub>	-1685.5326	0.5029	-1685.0297	0
-COOH ··· 1st-(H <sub>2</sub> O) <sub>4-vertical</sub>	-1685.5487	0.5055	-1685.0453	-8.45
-COOH ··· 1st-(H <sub>2</sub> O) <sub>4-horizontal</sub>	-1685.5608	0.5109	-1685.0517	-12.69
(-COOH + R-O-R) ··· 1st-(H <sub>2</sub> O) <sub>4</sub>	-1685.5534	0.5099	-1685.0455	-8.67
(-OH + -C = O) ··· 1st-(H <sub>2</sub> O) <sub>4</sub>	-1685.5538	0.5112	-1685.0460	-8.12
(-OH + -OH) ··· 1st-(H <sub>2</sub> O) <sub>4</sub>	-1685.5599	0.5113	-1685.0510	-11.86

**Fig. 6** Optimized structures of the adsorption of (a) water dimer, (b) water trimer, and (c) water tetramer on hydroxyl and carbonyl group



In conclusion, water monolayer can stably adsorb on the oxygen containing functional groups via H-bonds. Liu et al. [58] verified that water is easier to adsorb on oxygen containing functional groups by hydrothermal dewatering (HTD) experiment and a simple DFT study.

### Adsorption of multilayer water molecule

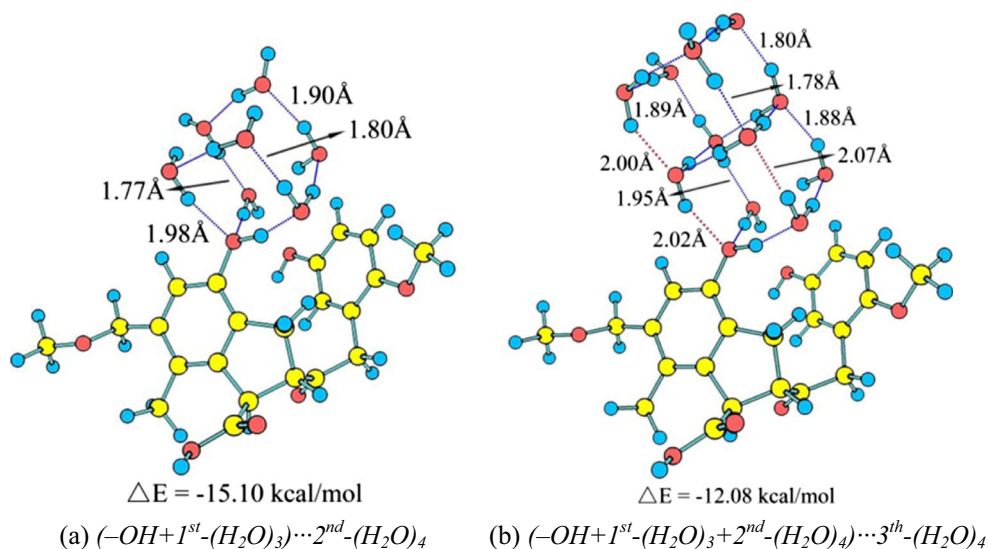
In actual environment, the adsorption of multilayer water molecule is interesting because both the hydrogen bonding of layers and water-lignite surface interactions are involved in the adsorbed water molecules. Furthermore, the adsorbed water, particularly the monolayer water, acts as “secondary sites” for the adsorption of additional free water, and thus generate cluster of water on the coal surface [24, 59]. Therefore, we build multilayer water models to simulate the influence of three-dimensional hydrogen bonding.

As shown in Fig. 7, water cluster can adsorb on hydroxyl functional group. First, hydroxyl group combines three free water molecules to form monolayer water in ring structure, and the mean of H-O distances in monolayer water structure is 1.79 Å. Then, water tetramer adsorbs on monolayer water via hydrogen bonding, and the average of adsorption distance is 1.86 Å. The bilayer water are formed in a stable cube structure. Finally, the other water tetramer adsorbs on the second layer water and the mean of adsorption distances is 1.87 Å. The hydroxyl group combines multilayer water molecules to

form a cubic configuration. Similarly, water clusters can adsorb on carboxyl functional group to form stable configurations as shown in Figs. 8 and 9, adsorb on both carboxyl and ether group as shown in Fig. 10, adsorb on two hydroxyl groups as shown in Fig. 11.

The mean of adsorption distances between the second and the first layer of water molecules are 1.86 Å, 2.03 Å, 1.84 Å, 1.90 Å, and 1.83 Å in Figs. 7a, 8a, 9a, 10a, and 11b, respectively. As shown in Table 4, the minimum and maximum adsorption energies of water tetramer bonding to the first layer water are  $(-COOH + 1^{st}-(H_2O)_2) \cdots 2^{nd}-(H_2O)_4$  and  $(-OH + -OH + 1^{st}-(H_2O)_4) \cdots 2^{nd}-(H_2O)_4$  configurations, respectively, and correspond to the longest and the shortest interaction distance between the second and the first layer water. Similarly, the values of adsorption energy of water tetramer adsorbs on the second layer water are negatively related to the interaction distances between the third and the second layer water. The correlation between interaction distance and adsorption energy of layers water is shown in Fig. 12. According to the analysis of Fig. 12, it can be found that the adsorption energy increases along with the decrease of interaction distance, and the correlation coefficients between interaction distance and adsorption energy of the second-first layer water and the third-second layer water are 0.95 and 0.76, respectively. Adsorption energies of the second layer water adsorbs on the first layer water are larger than that of the third-second layer water in general, and may be the reason

**Fig. 7** Optimized structures of the adsorption of multilayer water molecules on hydroxyl group



second layer water are closer to lignite surface than the third layer water, therefore, the lignite surface may attract the second layer water more strongly.

### Electrostatic potential on molecular surface

Electrostatic potential (ESP) on molecular van der Waals surface is virtual for studying and predicting intermolecular interaction [38, 60, 61], and it has been employed in characterizing various properties of some chemical systems [62–64]. In addition, electrostatic potential is well applicable in qualitative analysis, for which the ESP value provides a method to quantify reactivity at several specified positions in a molecule, both for intermolecular interactions like hydrogen bonding and for chemical reactions [61]. A comprehensive study of ESP of the adsorption configuration must be very helpful for deeper understanding of the interaction between lignite and water clusters. Hydrogen bonding is a typical and prominent non-covalent interaction, and that can be interpreted and predicted well with the electrostatic potential. The ESP on molecular

vdW surface and extreme points of lignite molecule are shown in Fig. 13, and the surface area in different ESP ranges are plotted as Fig. 14.

The lignite molecule is seen to have several regions of negative surface electrostatic potential, and these regions are associated with the lone pairs of the hydroxyl oxygen, ether oxygen, carbonyl oxygen and carboxyl oxygen, as well as with the  $\pi$  electrons of the carbon ring. As shown in Fig. 13, these negative regions overlap with each other, lone pair of each oxygen atom leads to one or more ESP minima on the lignite molecular surface, and the global surface minimum is  $-34.91$  kcal mol $^{-1}$  which is in the region of ether oxygen. Also, it is found that the electrostatic potential of benzene ring plane is less electronegative than that of lone pairs of oxygen atom. The ESP minimums of two benzene ring planes are  $-13.63$  kcal mol $^{-1}$  and  $-9.99$  kcal mol $^{-1}$ , respectively. The negative potential of hydroxyl oxygen lone pair is slightly lower than other oxygen atoms in functional groups. In contrast, there exist several regions of positive electrostatic potential as shown in white-mapped and red-mapped in Fig. 13.

**Fig. 8** Optimized structures of the adsorption of multilayer water molecules on carboxyl group (the first layer with two water)

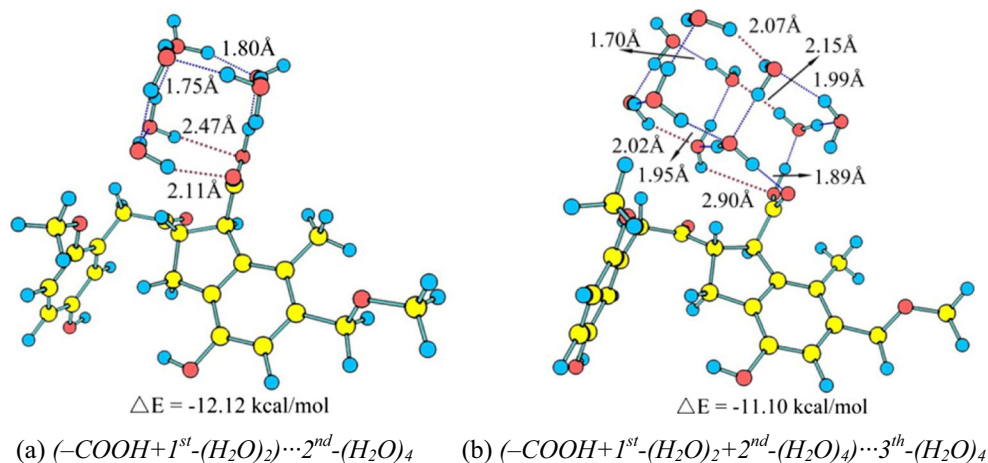
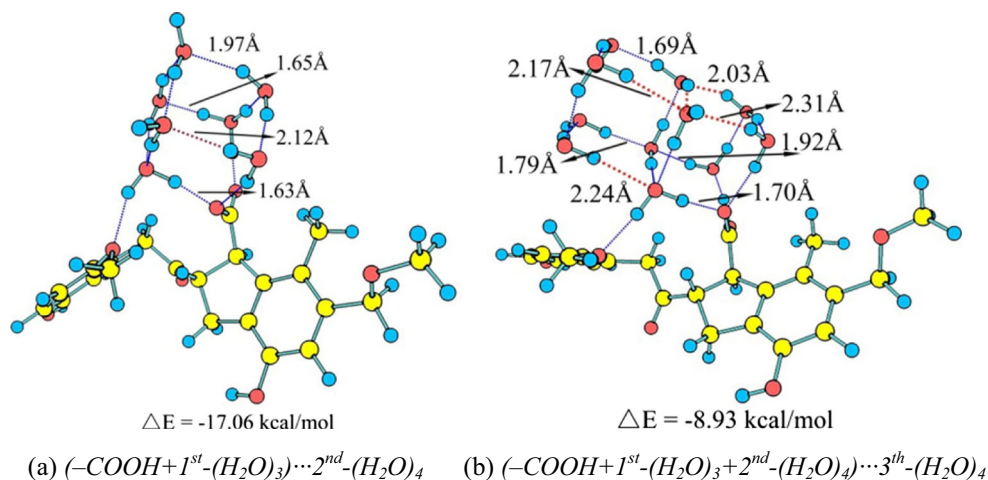


**Fig. 9** Optimized structures of the adsorption of multilayer water molecules on carboxyl group (the first layer with three water)



These positive electrostatic potential regions contain the carboxyl hydrogen and hydroxyl H atoms, and the value of the most positive one is  $47.55 \text{ kcal mol}^{-1}$ , which is also the global maximum. The value of the positive electrostatic potential of lignite surface region in a descending order is as follows: hydroxyl H, carboxyl hydrogen, benzene hydrogen, and branch hydrogen region. The maximum and minimum regions of surface electrostatic potential are easier to adsorb water molecules via hydrogen bonding or vdW interactions.

The molecular vdW surface can be partitioned into multiple fragments via the quantitative molecular surface analysis module of Multiwfn program [38], and these results can help us analyze the characteristic of ESP distribution of lignite molecule surface. From Fig. 14, it can be found that the largest surface area is  $127.41 \text{ \AA}^2$  for which the values of electrostatic potential are between  $-1.00$  and  $7.50 \text{ kcal mol}^{-1}$ . For the maximum and minimum electrostatic potential range, the molecular vdW surface areas are  $3.31 \text{ \AA}^2$  and  $19.04 \text{ \AA}^2$ , which occupy 0.79% and 4.55% of the overall surface, respectively. Only a small part of the lignite surface has a large absolute ESP value, which corresponds to the oxygen containing functional group regions with strong polarity. The positive ESP regions are larger than the negative ESP regions in general, reflecting the proportion of hydrogen regions are greater than

that of  $\pi$ -cloud of the carbons and oxygen regions of functional groups.

The lignite molecule has some regions of positive and negative electrostatic potential, in which are found one or more local minima and maxima, and these regions are easier to adsorb free water molecules. Figure 15 shows typical conformations of multilayer water molecules adsorb on carboxyl group in lignite. It is found that the electrostatic potential area of configuration becomes greater along with more water molecules adsorbing on lignite. More local maxima and minima appear around hydrogen and oxygen atoms of adsorbed water molecules, respectively. Except carboxyl group area, the adsorbed water clusters have little effect on electrostatic potential of lignite surface. Considering water is a polar molecule, the adsorption of water molecules can result in producing more adsorption sites with local minima and maxima of electrostatic potential. As shown in Fig. 15, the local ESP value of hydrogen in adsorbed water is close to that of functional group hydrogen and significantly larger than that of branch hydrogen. Comparing Figs. 13 and 15b, the local minima and maxima of electrostatic potential in the region of carboxyl group increased along with water dimer adsorbs on carboxyl in lignite. Similarly, the adsorption of water tetramer on the monolayer and the second layer water leads to more local minima

**Fig. 10** Optimized structures of the adsorption of multilayer water molecules on carboxyl group and ether bond

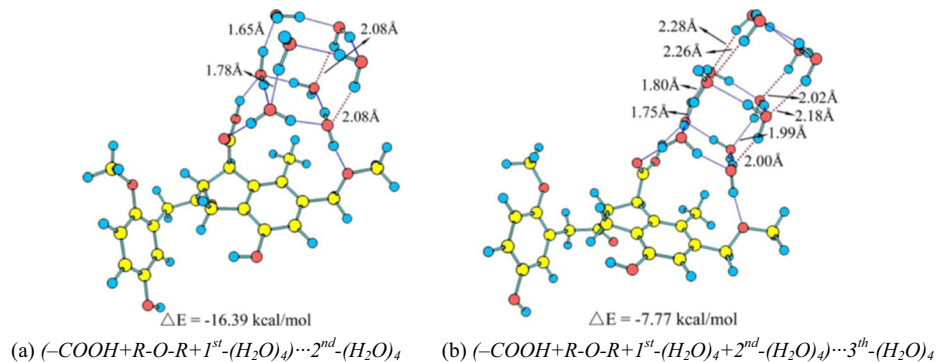


**Fig. 11** Optimized structures of the adsorption of multilayer water molecules on two hydroxyl groups

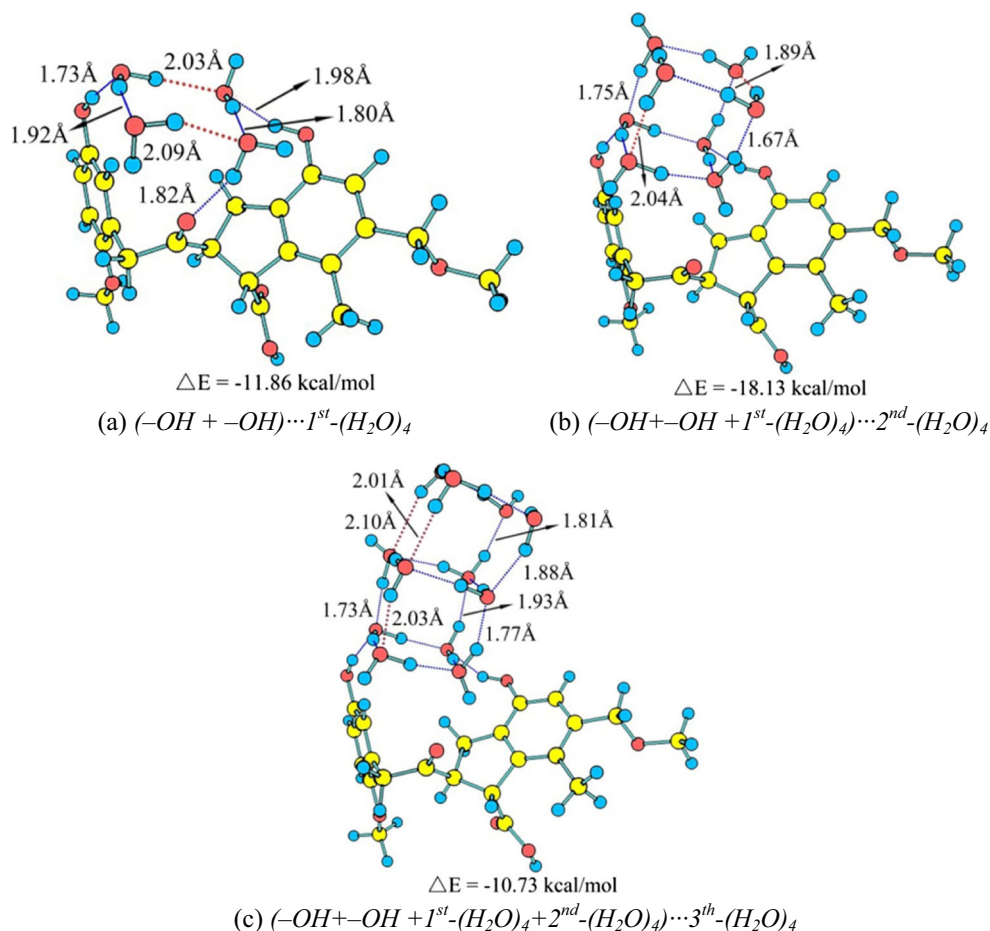


**Table 4** Interaction energy of the multilayer water adsorbs on lignite surface<sup>a</sup>

Configurations	$(-OH + 1^{st}-(H_2O)_3)$	$(-OH + 1^{st}-(H_2O)_3 +$
$-OH \cdots 1^{st}-(H_2O)_3 + (H_2O)_4$	$\cdots 2^{nd}-(H_2O)_4$	$2^{nd}-(H_2O)_4) \cdots 3^{th}-(H_2O)_4$
$(-OH + 1^{st}-(H_2O)_3) \cdots 2^{nd}-(H_2O)_4 + (H_2O)_4$	-15.10	-
	-	-12.08
Configurations	$(-COOH + 1^{st}-(H_2O)_2)$	$(-COOH + 1^{st}-(H_2O)_2 +$
$-COOH \cdots 1^{st}-(H_2O)_2 + (H_2O)_4$	$\cdots 2^{nd}-(H_2O)_4$	$2^{nd}-(H_2O)_4) \cdots 3^{th}-(H_2O)_4$
$(-COOH + 1^{st}-(H_2O)_2) \cdots 2^{nd}-(H_2O)_4 + (H_2O)_4$	-12.12	-
	-	-11.10
Configurations	$(-COOH + 1^{st}-(H_2O)_3)$	$(-COOH + 1^{st}-(H_2O)_3 +$
$-COOH \cdots 1^{st}-(H_2O)_3 + (H_2O)_4$	$\cdots 2^{nd}-(H_2O)_4$	$2^{nd}-(H_2O)_4) \cdots 3^{th}-(H_2O)_4$
$(-COOH + 1^{st}-(H_2O)_3) \cdots 2^{nd}-(H_2O)_4 + (H_2O)_4$	-17.06	-
	-	-8.93
Configurations	$(-COOH + R-O-R +$	$(-COOH + R-O-R + 1^{st}-(H_2O)_4$
$-COOH + R-O-R + 1^{st}-(H_2O)_4) + (H_2O)_4$	$1^{st}-(H_2O)_4) \cdots 2^{nd}-(H_2O)_4$	$+ 2^{nd}-(H_2O)_4) \cdots 3^{th}-(H_2O)_4$
$(-COOH + R-O-R + 1^{st}-(H_2O)_4) \cdots 2^{nd}-(H_2O)_4 + (H_2O)_4$	-16.39	-
	-	-7.77
Configurations	$(-OH + -OH + 1^{st}-(H_2O)_4)$	$(-OH + -OH + 1^{st}-(H_2O)_4 +$
$-OH + -OH) \cdots 1^{st}-(H_2O)_4 + (H_2O)_4$	$\cdots 2^{nd}-(H_2O)_4$	$2^{nd}-(H_2O)_4) \cdots 3^{th}-(H_2O)_4$
$(-OH + -OH + 1^{st}-(H_2O)_4) \cdots 2^{nd}-(H_2O)_4 + (H_2O)_4$	-18.13	-
	-	-10.73

The values in table are obtained via energy of the first column configurations subtracted from other columns configurations

<sup>a</sup> Energy is in kcal mol<sup>-1</sup>

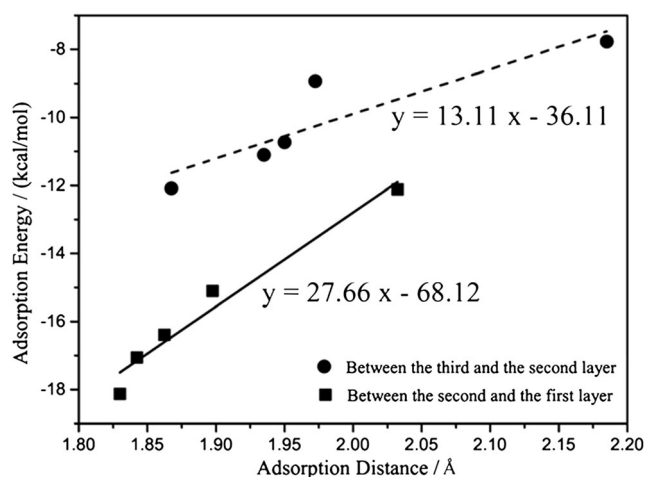


**Fig. 12** The correlation between interaction distance and adsorption energy of water layers. *Dots* represent the third-layer water molecules adsorb on the second-layer water; *blocks* represent the second-layer water molecules adsorb on the first-layer water

and maxima of electrostatic potential, respectively as shown in Fig. 15c and d. From Fig. 15, it can be found that the hydrogen atom which is not involved in forming hydrogen bond in adsorbed water represents great positive electrostatic potential, such as the local ESP value of 42.88 kcal mol<sup>-1</sup> of hydrogen atom region in Fig. 15a. These hydrogen atoms which are not part of hydrogen bonding can produce local ESP maxima, therefore, these hydrogen atoms in adsorbed water more easily adsorb more free water molecules.

As shown in Fig. 16, in general, surface area in each ESP range increases along with more water molecules adsorb on lignite. Surface area in large positive value (above 36 kcal mol<sup>-1</sup>) of ESP range occupies 1.79%, 1.99%, 3.38%, and 5.71% in  $-COOH \cdots 1st-H_2O$ ,  $-COOH \cdots 1st-(H_2O)_2$ ,  $(-COOH + 1st-(H_2O)_2) \cdots 2nd-(H_2O)_4$  and  $(-COOH + 1st-(H_2O)_2 + 2nd-(H_2O)_4) \cdots 3th-(H_2O)_4$  configurations, respectively. Similarly, surface area in large negative value (below -30 kcal mol<sup>-1</sup>) of ESP range represents 4.38%, 1.63%, 1.61%, and 2.02% of the total surface for four configurations mentioned above. The proportion of surface region with large

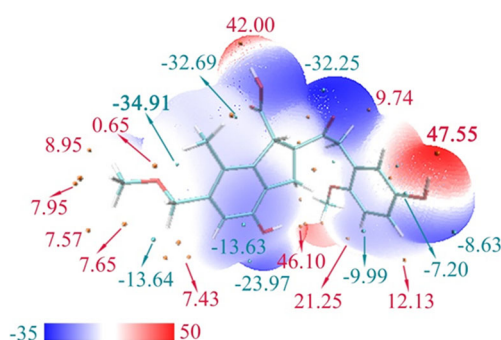


**Fig. 13** ESP on the molecular surface of lignite. The unit is kcal mol<sup>-1</sup> and local minima and maxima of ESP are represented as *cyan* and *orange* spheres, respectively. The global minimum and maximum are labeled by bold font

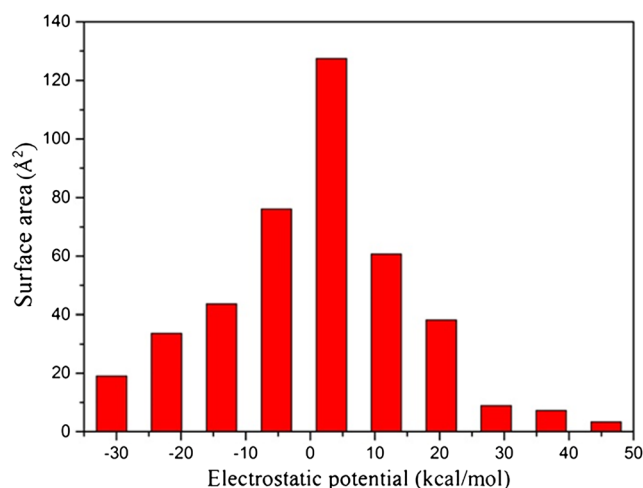


**Fig. 14** Surface area in each ESP range on the molecular surface of lignite

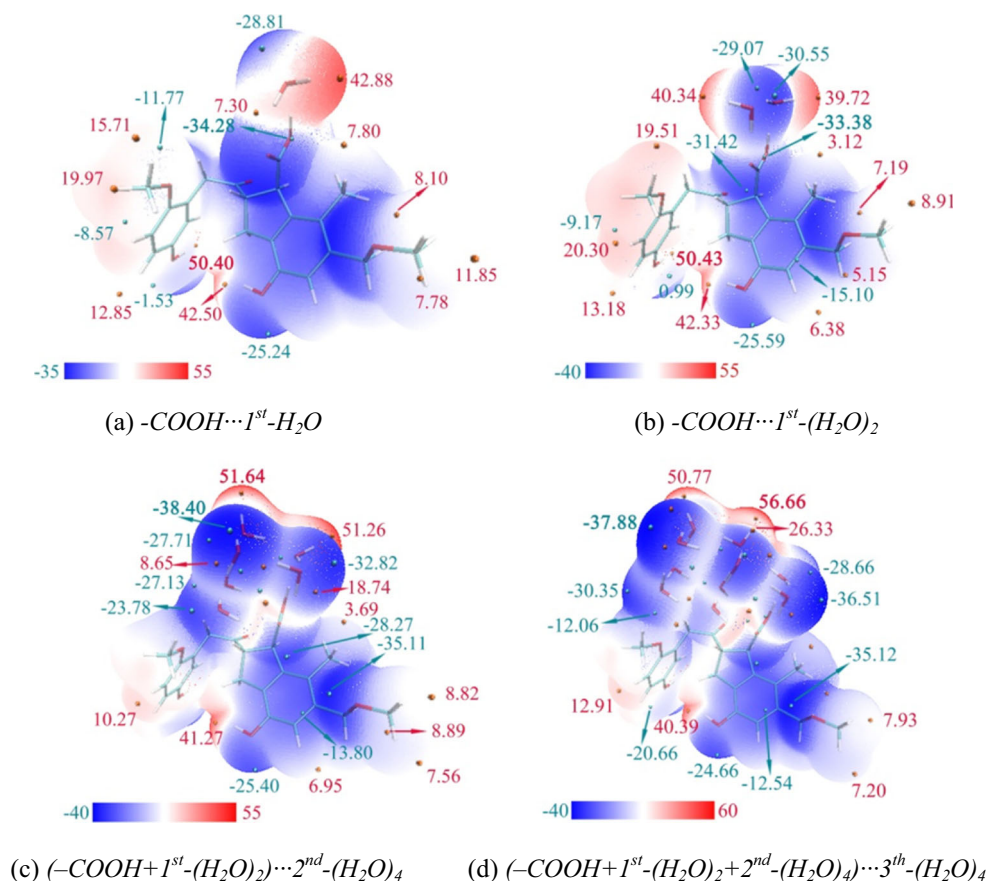
positive value increases along with the adsorption of water molecules, and qualitatively, it indicates that adsorption capacity of lignite is enhanced due to water molecules adsorb on lignite surface. The value of the ESP ranges from 0 to 10 kcal mol<sup>-1</sup> in these four adsorption configurations has the largest surface area, these ESP areas are 149.73 Å<sup>2</sup>, 153.74 Å<sup>2</sup>, 166.85 Å<sup>2</sup>, and 180.34 Å<sup>2</sup>, respectively, and they occupy 33.44%, 32.53%, 32.03%, and 30.55% of the overall surface. Comparing Figs. 14 and 16, it is shown that the distribution of different ESP ranges of adsorption geometries is similar to that of lignite molecule.

### RDG analysis of water $\cdots$ lignite complex

Reactions between water and lignite molecule are dominated by non-covalent interactions. The class of these interactions spans a wide range of hydrogen bonding, dispersion interactions, and steric repulsion [44, 65]. Intermolecular H-bond is the most notable bond of water  $\cdots$  lignite complexes, which affects stability among various adsorption conformations. Reduced density gradient (RDG) analysis method [44] was applied for deeper study and give a more intuitive picture for these kinds of interactions. RDG analysis is an ideal method for revealing non-covalent interactions [66], we carried out RDG analysis for typical conformations in which water adsorbs on carboxyl group in lignite, and gradient isosurfaces and corresponding scatter plots of RDG versus  $\text{sign}(\lambda_2)\rho$  for configurations, as shown in Fig. 17.

The sign of  $\lambda_2$  can be used to distinguish bonded ( $\lambda_2 < 0$ ) from nonbonded ( $\lambda_2 > 0$ ) interactions, whereas the electron density  $\rho$  provides information about their strength [44]. Large negative and positive values of  $\text{sign}(\lambda_2)\rho$  are indicative of attractive and repulsive interactions, respectively. In the scatter plots,  $\text{sign}(\lambda_2)\rho$  spikes lying at large negative values indicate stably attractive interaction, such as hydrogen bond

**Fig. 15** ESP on the molecular surface of lignite adsorbing (a) one water molecule, (b) two water molecules, (c) six water molecules, and (d) ten water molecules. The unit is in kcal mol<sup>-1</sup> and local minima and maxima of ESP are represented as cyan and orange spheres, respectively. The global minimum and maximum are labeled by bold font



and halogen bond.  $Sign(\lambda_2)\rho$  spikes lying at near zero values indicate weak attraction, like van der Waals interaction. Conversely,  $sign(\lambda_2)\rho$  spikes lying at large positive values indicate strong repulsion, such as steric.

In Fig. 17a1–d1, water cluster and carboxyl group regions enclosed by the RDG isosurface with value 0.50, the mapped color shows position and type of weak interaction. As shown in Fig. 17a1, the isolated water

molecule adsorbs on carboxyl group via strong H-bond (navy blue isosurface) and van der Waals interaction (green isosurface), also there exist repulsion interaction (orange isosurface) between water and carboxyl group, which is similar to that given by Wu et al. [54]. Among these interactions, strong H-bond corresponds to  $sign(\lambda_2)\rho$  spikes lying at negative values (below  $-0.025$ ) in Fig. 17a2; and weak van der Waals interaction corresponds to a spike lying at near the origin; steric interaction corresponds to a spike lying at positive values. In Fig. 17b1, it is intuitively found that there are three H-bonds forming between water dimer and carboxyl group, corresponding to the color-filled RDG map in navy blue and  $sign(\lambda_2)\rho$  spikes lying at large negative values, which indicates that the strength of H-bond is strong. Also, steric effect presents in the center of the ring of water dimer and carboxyl group. Comparing among Fig. 17b1, c1, and d1, it is shown that interactions between water layers are mainly H-bonds and van der Waals interaction, steric exists in both the center of the water tetramer ring and water cluster cube. Therefore, it is concluded that the structure of water  $\cdots$  lignite complex is influenced by attractive and repulsive interactions, H-bonds play a dominant role in the formation of these conformations.

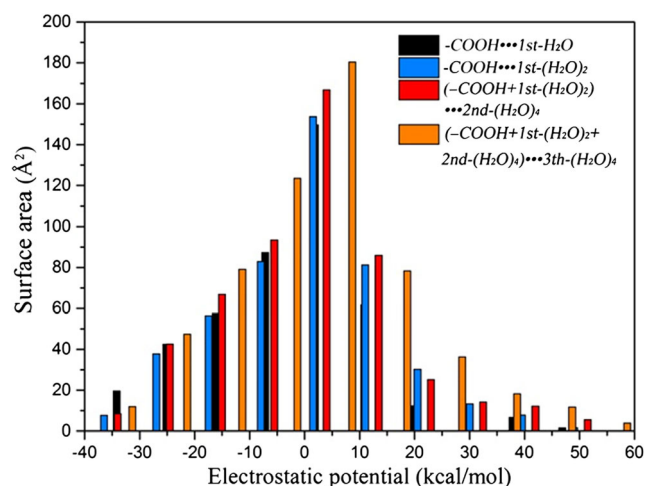
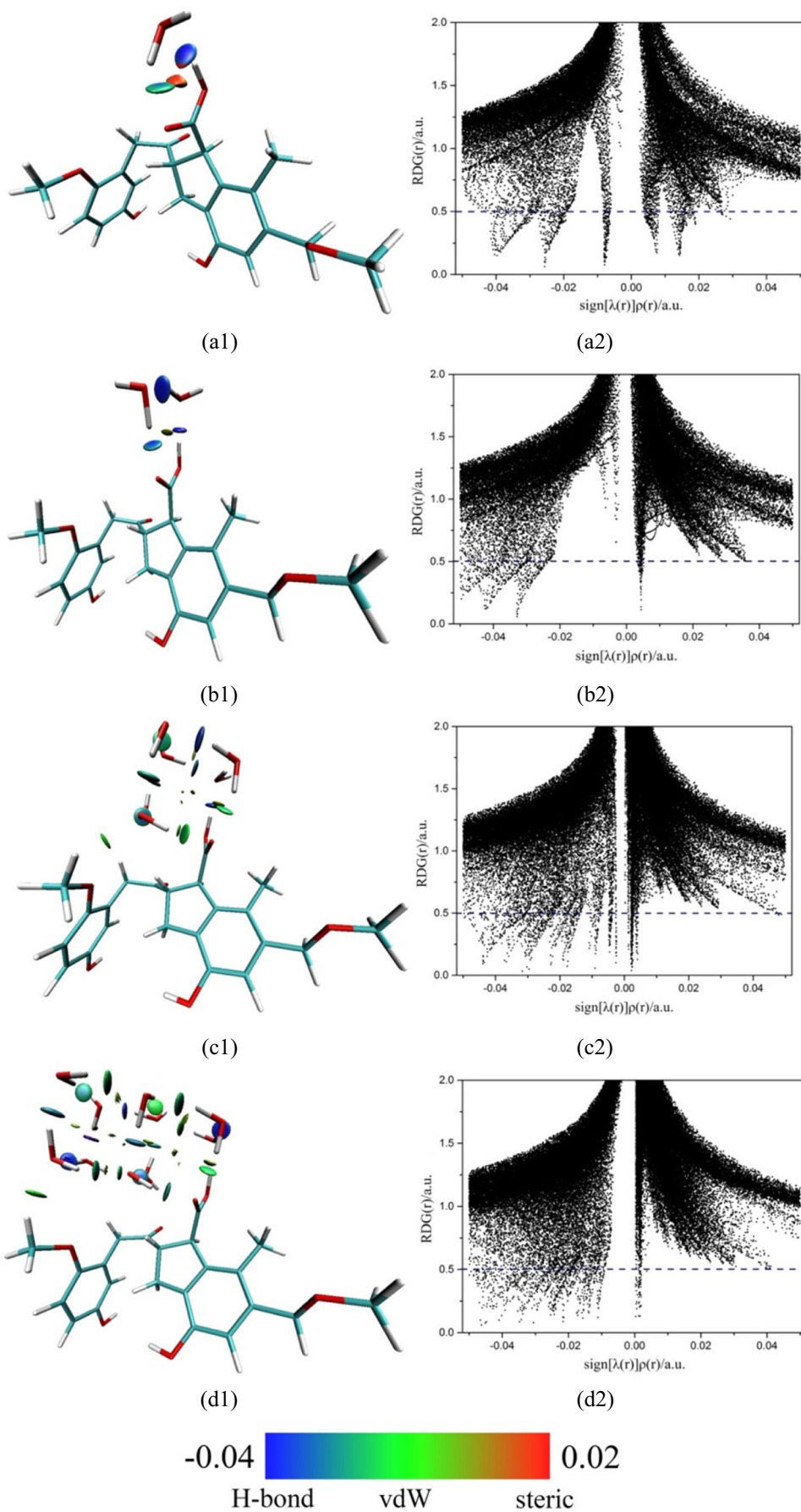


**Fig. 16** Surface areas in each ESP range on the molecular surface of different configurations



◀ **Fig. 17** Color-filled reduced density gradient (RDG) map of optimized conformations and corresponding scatter plots: (a)  $-COOH \cdots 1st-H_2O$ ; (b)  $-COOH \cdots 1st-(H_2O)_2$ ; (c)  $(-COOH + 1st-(H_2O)_2) \cdots 2nd-(H_2O)_4$ ; (d)  $(-COOH + 1st-(H_2O)_2 + 2nd-(H_2O)_4) \cdots 3th-(H_2O)_4$ . The value of isosurface of RDG is set to 0.5. The value of  $sign(\lambda_2)\rho$  on the surfaces is represented by filling color according to the color bar at bottom. Scatter plots of reduced density gradient (RDG) versus electron density ( $\rho$ ) multiplied by the sign of the second Hessian eigenvalue ( $\lambda_2$ )

### Energy decomposition analysis of water $\cdots$ lignite complex

Energy decomposition analysis (EDA) method is widely used in studying weak interaction, and it can provide insights into intermolecular interactions by separating the total interaction energy into various terms such as electrostatic, exchange, repulsion, polarization, and dispersion energy. Electrostatic interaction results from the undistorted electron distribution of two monomers, this interaction may be either attractive or repulsive. Exchange repulsion interaction caused by exchange of electrons between two monomers, and this interaction is the short-range repulsion due to overlap of electron distribution. Polarization interaction which is caused by the effect of distortion of the electron distribution for two monomers, this interaction is always attractive [67]. Dispersion is the interaction of two neutral monomers with a non-overlapping charge density, that dispersion interaction is always attractive [68, 69].

The various terms of energy of some water  $\cdots$  lignite complexes are listed in Table 5. EDA was carried out at the BLYP/6-31+G(d,p) level, and dispersion energy was obtained via ORCA at the BLYP-D3/6-31+G(d,p) level, and the reference total interaction energy was calculated at the PWPB95-D3/def2-QZVPP(-g, -f) level.

In Table 5, it is found that the value of  $\Delta E_{BSSE}$  is greater than  $1.00 \text{ kcal mol}^{-1}$  in all conformations, particularly in  $(-OH + -C = O) \cdots 1st-H_2O$  as shown in Fig. 2d, the value of  $\Delta E_{BSSE}$  accounts for half  $E_{total}$ . It indicates that BSSE correction is crucial in calculating weak interaction energy.

The interaction energy components of single water adsorbs on lignite surface as shown in the first four rows in Table 5 and Fig. 18. The electrostatic energy of single water adsorbs on carboxyl group is larger than that of other conformations, the minimum value of electrostatic energy is  $-12.67 \text{ kcal mol}^{-1}$  for water bonding with carboxyl and ether groups. Change trend of polarization energy value (blue line) similar to electrostatic energy value (black line) as shown in Fig. 18, and large values of the sum of electrostatic and polarization energy represent strong attractive interaction. Compared with the other conformations, the shortest H-bond length in  $-COOH \cdots 1st-H_2O$  contributes to the strong attractive interaction between atoms O1 and H3 in the conformation with large value of electrostatic and polarization energy. Also color-filled RDG map of  $-COOH \cdots 1st-H_2O$  conformation as shown in

Fig. 17a1, the color-filled RDG map shows that steric repulsion interaction exists between water molecule and carboxyl group, thus the repulsion energy is relatively large. Comparing Fig. 2c and d, the mean length of  $O2 \cdots H1$  and  $O3 \cdots H2$  versus  $O2 \cdots H1$  and  $O1 \cdots H3$  are approximately equal, the value of electrostatic and polarization energy components are also roughly equal. Dispersion energy of these four conformations is relatively small which indicates that long-range interaction plays a weak role in the adsorption of single water on lignite surface. Among all energy components of water  $\cdots$  lignite complexes which single water directly adsorbs on lignite, exchange repulsion energy is almost equal to or even slightly larger than electrostatic energy, the contribution of polarization and dispersion energy are small.

The energy components of water polymer adsorbed on carboxyl group in Fig. 19 correspond to configurations which are shown in Fig. 4. In  $-COOH \cdots 1st-(H_2O)_4$ -horizontal conformation, water tetramer horizontally adsorbs on lignite surface in contrast to vertically adsorb as shown in Fig. 4c. Comparing Fig. 4a and b, the mean lengths of  $O3 \cdots H1$  and  $O2 \cdots H5$  are slightly shorter than that of  $O5 \cdots H1$  and  $O3 \cdots H7$ , which correspond to larger electrostatic and polarization energy in  $-COOH \cdots 1st-(H_2O)_2$  configuration. However, in  $-COOH \cdots 1st-(H_2O)_4$ -vertical configuration, the mean length of  $O1 \cdots H1$  and  $O2 \cdots H2$  is longer than that of  $-COOH \cdots 1st-(H_2O)_3$  configuration, the electrostatic and polarization energy are larger than that of  $-COOH \cdots 1st-(H_2O)_3$  conformation. It indicates that interaction distance is not the only factor which affects interaction energy components of water molecules directly adsorbed on lignite surface, the bond angle and spatial location of water molecules may be the other factors. The electrostatic energy of the water tetramer that horizontally adsorbs on lignite surface is greater than that of vertically adsorb, because adsorbing horizontally can make water tetramer closer to lignite surface and more atoms can be involved in interacting. Dispersion energy of these conformations is little, which qualitatively indicates that dispersion interaction makes less contribution to water clusters directly adsorbed on lignite surface.

The interaction energy components of water tetramer adsorbs on the first water layer and the second water layer are shown in Fig. 20a and b, respectively. It is shown that electrostatic and exchange repulsion energy of  $3th \cdots 2nd$  water layer conformations are less than that of  $2nd \cdots 1st$  water layer conformations in general. Except for  $(-COOH + 1st-(H_2O)_2) \cdots 2nd-(H_2O)_4$  conformation as shown in Fig. 8, in other conformations, the interaction distances between the third water layer and the second layer are slightly longer than that between the second layer and the first layer. It indicates that interaction distance relates to the electrostatic and exchange repulsion energy component between the adsorbed water layers. Comparing Figs. 19 and 20, it is found that dispersion energy of  $2nd \cdots 1st$  water layer and  $3th \cdots 2nd$  water layer conformations is slightly larger than that of

**Table 5** EDA of the water  $\cdots$  lignite complexes<sup>a</sup>

Conformations	$E_{\text{ele}}$	$E_{\text{ex}}$	$E_{\text{rep}}$	$E_{\text{pol}}$	$E_{\text{disp}}$	$E_{\text{other}}$	$E_{\text{total}}$	$\Delta E_{\text{BSSE}}$	$E_{\text{total}}^{\text{'}}$
Fig. 2a	-15.73	-2.03	18.85	-4.94	-2.83	-2.08	-8.76	1.53	-6.21
Fig. 2b	-23.5	-7.46	33.54	-8.77	-1.64	-2.34	-10.17	1.02	-6.68
Fig. 2c	-12.67	-8.64	24.08	-2.47	-4.52	-2.85	-7.07	1.24	-4.66
Fig. 2d	-14.11	-3.87	20.26	-2.14	-3.47	-2.64	-5.97	1.16	-2.25
Fig. 4a	-32.02	-8.79	46.31	-18.46	-2.61	-2.1	-17.67	1.5	-12.9
Fig. 4b	-23.92	-9.61	43.52	-14.41	-3.57	-4.65	-12.64	2.35	-9.7
Fig. 4c	-27.3	-7.02	41.1	-12.86	-2.68	-2.99	-11.75	371	-8.45
Fig. 4d	-37.9	-10.04	50.52	-11.45	-5.45	-2.61	-16.93	3.36	-12.69
Fig. 7a	-45.02	-15.3	65.18	-11.76	-9.73	-4.34	-20.97	3.21	-15.1
Fig. 8a	-37.47	-12.1	57.16	-10.32	-8.77	-4.4	-15.9	3.48	-12.12
Fig. 9a	-47.98	-17.02	68.22	-12.22	-8.54	-3.35	-20.89	4.21	-17.06
Fig. 10a	-46.87	-14.64	66.26	-11.9	-10.45	-4.25	-21.85	4.11	-16.39
Fig. 11b	-48.54	-16.83	65.34	-13.18	-7.68	-3.25	-24.14	4.19	-18.13
Fig. 7b	-38.45	-14.43	60.04	-10.12	-7.5	-5.98	-16.44	3.96	-12.08
Fig. 8b	-35.09	-15.85	58.74	-9.43	-8.47	-3.56	-13.66	3.87	-11.10
Fig. 9b	-30.28	-15.68	53.98	-8.49	-8.26	-2.93	-11.66	2.76	-8.93
Fig. 10b	-26.8	-11.5	45.45	-5.09	-7.24	-5.4	-10.58	2.69	-7.77
Fig. 11c	-33.05	-14.31	57.89	-9.74	-7.9	-4.28	-11.39	3.08	-10.73

$E_{\text{ele}}$  is electrostatic energy;  $E_{\text{ex}}$  is exchange energy;  $E_{\text{rep}}$  is repulsion energy;  $E_{\text{pol}}$  is polarization energy;  $E_{\text{disp}}$  is dispersion energy obtained via ORCA program at BLYP-D3/6-31+G(d,p) level;  $E_{\text{other}}$  is “dispersion energy” obtained via LMO-EDA program at BLYP/6-31+G(d,p) level;  $E_{\text{total}}$  is the sum of  $E_{\text{ele}}$ ,  $E_{\text{ex}}$ ,  $E_{\text{rep}}$ ,  $E_{\text{pol}}$ ,  $E_{\text{disp}}$ , and  $E_{\text{other}}$ ;  $\Delta E_{\text{BSSE}}$  is the difference of  $E_{\text{total}}$  which involves BSSE correction and  $E_{\text{total}}^{\text{'}}$  with no BSSE correction;  $E_{\text{total}}^{\text{'}}$  is the reference energy which can be calculated at high level of basis set

<sup>a</sup> Energy is in kcal mol<sup>-1</sup>

conformations in Fig. 19. As shown in Fig. 17, a color-filled RDG map of typical conformations of water clusters adsorb on carboxyl group, H-bonds and vdW interactions increase along with the adsorption of more water tetramer on lignite surface, and dispersion is a dominant component of vdW interaction in most complexes. Therefore, in *2nd*  $\cdots$  *1st* water layer and *3th*  $\cdots$  *2nd* water layer conformations, high vdW interactions lead to increase of dispersion energy, and the dispersion interaction makes more contribution to the adsorption

of water clusters on lignite surface. After one or two adsorption layers of water are formed, dispersion forces play a more important role in the further adsorption of water layers [70]. When the water cluster is located in pores equal to its size, it may also slightly enhance the adsorption energy due to dispersive interactions with the pore walls [53]. And water cluster entities have enough dispersion energy to be released from hydrophilic groups and to be adsorbed on the hydrophobic carbon surface [71]. Stated thus, the adsorption of water

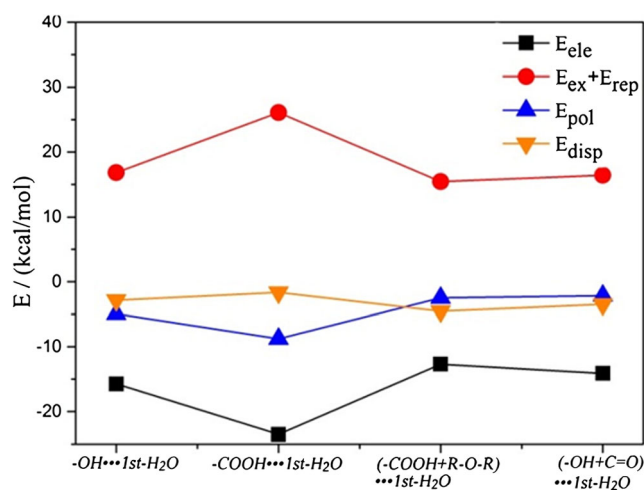


**Fig. 18** Adsorption energy components of single water on lignite surface

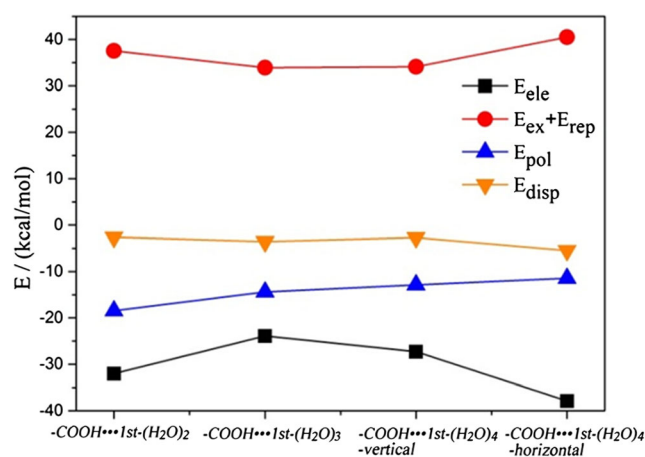


**Fig. 19** Adsorption energy components of water polymers on carboxyl group

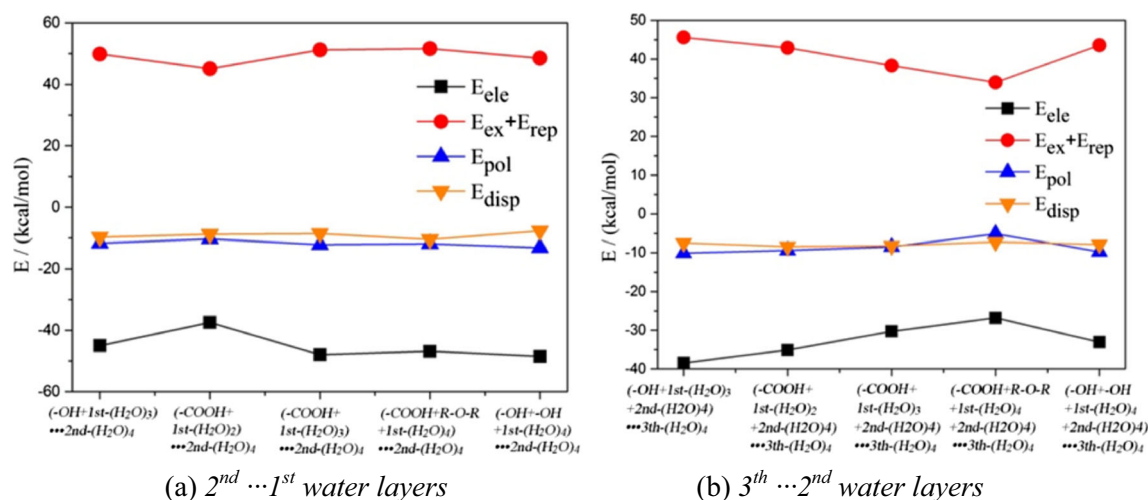


**Fig. 20** Adsorption energy components of (a) the second water tetramer layer on the first water layer surface, (b) the third water tetramer layer on the second water layer surface

clusters on lignite surface is affected by attractive and repulsive interaction.

## Conclusions

Lignite is an important coal variety with high moisture content. To afford more knowledge on the adsorption mechanisms of water molecules on lignite surface, in this study, some typical adsorption conformations are investigated.

By applying DFT theory, the influence of oxygen containing functional groups on water adsorbing is analyzed. To simulate relative, actual existing mechanisms of water molecules on lignite surface, the adsorption of multilayer water on lignite surface is also studied.

Electrostatic surface potential (ESP) of lignite molecule model and some typical equilibrium configurations are evaluated to predict the adsorption sites of water molecule on lignite surface. RDG is applied for the analysis and visualization of the interaction between water molecule and lignite. Moreover the interaction energy of water  $\cdots$  lignite complexes are decomposed into several terms at relatively low basis set level for qualitative analysis.

DFT analysis shows that, compared to the other components in coal, e.g., benzene ring and aliphatic hydrocarbon chain, isolated water or water clusters are more easily adsorbed on functional group surface. Also, isolated water adsorbed on functional group can promote the adsorption of other free water via providing hydrogen atom as H-bond acceptor or oxygen atom as H-bond donor.

Among all the functional groups, the conformation in which isolated water is adsorbed on carboxyl group is the most stable one. On the other hand, the water dimer and multilayer water are both more easily adsorbed on lignite surface than isolated water. A good linear relationship between the

interaction distance and interaction energy of water layers is detected in this study.

ESP analysis shows that hydrogen and oxygen atom in functional group represent local maximum positive and negative electrostatic potential respectively, strongly attracting some polar molecules. The number of local minimum and maximum points of electrostatic potential in conformations increase along with more water molecules adsorbing on lignite surface, probably contributing to more water molecules getting adsorbed.

RDG analysis shows that interactions between water clusters and lignite molecule mainly are H-bond, van der Waals interaction, and a little steric. Along with the number of water increasing layers, vdW interaction makes more contribution to the interaction between water layers and lignite molecule.

Energy decomposition analysis (EDA) shows that electrostatic and exchange repulsion play a dominant role in the interaction of water  $\cdots$  lignite complexes, polarization and dispersion make relatively small contribution to the adsorption, indicating that water molecule gets adsorbed on lignite surface mainly through electrostatic attraction. Attractive and repulsive interaction both affect the stability of water  $\cdots$  lignite complexes.

The adsorption of single water molecule, water dimer, and multilayer water on functional groups discussed above are the main interactions of the adsorption mechanism of water molecule on lignite surface; these adsorption mechanisms well explain the reason for high moisture content characteristic of low-rank lignite. During coal drying, compared with other high-rank coal, considering the strong interactions between water molecule and lignite surface, drying requires much more energy consumption and better condition of moisture diffusion. In addition, large numbers of local maximum and minimum points around functional groups make relapse of water adsorption occur easily. Thus, lignite

should be stored in a dry environment after drying to prevent adsorption relapse.

## References

- Zhang Y, Schauer JJ, Zhang Y, Zeng L, Wei Y, Liu Y, Shao M (2008) Characteristics of particulate carbon emissions from real-world Chinese coal combustion. *Environ Sci Technol* 42(14):5068–5073
- Thielemann T, Schmidt S, Gerling JP (2007) Lignite and hard coal: energy suppliers for world needs until the year 2100—An outlook. *Int J Coal Geol* 72(1):1–14
- Allardice DJ (1991) The water in brown coal. In: Durie RA (ed) *The science of victorian brown coal: structure, properties and consequence for utilization*, Butterworth-Heinemann, Oxford, pp 103–150
- Jia R, Harris GH, Fuerstenau DW (2000) An improved class of universal collectors for the flotation of oxidized and/or low-rank coal. *Int J Miner Process* 58(1):99–118
- Karthikeyan M, Kuma JV, Hoe CS, Ngo DLY (2007) Factors affecting quality of dried low-rank coals. *Dry Technol* 25(10):1601–1611
- Tahmasebi A, Yu J, Han Y, Zhao H, Bhattacharya S (2013) Thermogravimetric study and modeling for the drying of a Chinese lignite. *Asia Pac J Chem Eng* 8(6):793–803
- Karthikeyan M, Zhonghua W, Mujumdar AS (2009) Low-rank coal drying technologies—current status and new developments. *Dry Technol* 27(3):403–415
- Salmas CE, Tsetsekou AH, Hatzilyberis KS, Androutsopoulos GP (2001) Evolution lignite mesopore structure during drying. Effect of temperature and heating time. *Dry Technol* 19(1):35–64
- Murata S, Hosokawa M, Kidena K, Nomura M (2000) Analysis of oxygen-functional groups in brown coals. *Fuel Process Technol* 67(3):231–243
- Ogunsola OI (1993) Thermal upgrading effect on oxygen distribution in lignite. *Fuel Process Technol* 34(1):73–81
- Deevi SC, Suuberg EM (1987) Physical changes accompanying drying of western US lignites. *Fuel* 66(4):454–460
- Suuberg EM, Otake Y, Yun Y, Deevi SC (1993) Role of moisture in coal structure and the effects of drying upon the accessibility of coal structure. *Energy Fuel* 7(3):384–392
- Murray JA, Evans DG (1972) The brown-coal/water system: Part 3. Thermal dewatering of brown coal. *Fuel* 51(4):290–296
- Franks F (2013) *Water a comprehensive treatise: volume 4: aqueous solutions of amphiphiles and macromolecules*. Springer Science & Business Media
- Qi N, LeVan MD (2005) Adsorption equilibrium modeling for water on activated carbons. *Carbon* 43(11):2258–2263
- Zimny T, Finqueneisel G, Cossarutto L, Weber JV (2005) Water vapor adsorption on activated carbon preadsorbed with naphthalene. *J Colloid Interface Sci* 285(1):56–60
- Carlson HR (1979) Do clusters contribute to the infrared absorption spectrum of water vapor? *Infrared Phys* 19(5):549–557
- Švábová M, Weishauptová Z, Příbyl O (2011) Water vapour adsorption on coal. *Fuel* 90(5):1892–1899
- Arisoy A, Akgün F (1994) Modelling of spontaneous combustion of coal with moisture content included. *Fuel* 73(2):281–286
- Yu J, Tahmasebi A, Han Y, Yin F, Li X (2013) A review on water in low rank coals: the existence, interaction with coal structure and effects on coal utilization. *Fuel Process Technol* 106:9–20
- Fletcher AJ, Uygur Y, Thomas KM (2007) Role of surface functional groups in the adsorption kinetics of water vapor on microporous activated carbons. *J Phys Chem C* 111(23):8349–8359
- Kaji R, Muranaka Y, Otsuka K, Hishinuma Y (1986) Water absorption by coals: effects of pore structure and surface oxygen. *Fuel* 65(2):288–291
- Nishino J (2001) Adsorption of water vapor and carbon dioxide at carboxylic functional groups on the surface of coal. *Fuel* 80(5):757–764
- McCutcheon AL, Barton WA, Wilson MA (2003) Characterization of water adsorbed on bituminous coals. *Energy Fuel* 17(1):107–112
- Charrière D, Behra P (2010) Water sorption on coals. *J Colloid Interface Sci* 344(2):460–467
- Kumagai H, Hayashi J, Chiba T, Nakamura K (1999) Change in physical and chemical characteristics of brown coal along with a progress of moisture release. In: *Abstracts of papers of the American Chemical Society*, vol. 218. Amer Chemical Soc, Washington, DC, pp U611–U611
- Vu T, Chaffee A, Yarovsky I (2002) Investigation of lignin-water interactions by molecular simulation. *Mol Simul* 28(10–11):981–991
- Stephens PJ, Devlin FJ, Chabalowski C, Frisch MJ (1994) Ab initio calculation of vibrational absorption and circular dichroism spectra using density functional force fields. *J Phys Chem* 98(45):11623–11627
- Grimme S, Ehrlich S, Goerigk L (2011) Effect of the damping function in dispersion corrected density functional theory. *J Comput Chem* 32(7):1456–1465
- Kruse H, Grimme S (2012) A geometrical correction for the inter- and intra-molecular basis set superposition error in Hartree-Fock and density functional theory calculations for large systems. *J Chem Phys* 136(15):154101
- Weigend F, Ahlrichs R (2005) Balanced basis sets of split valence, triple zeta valence and quadruple zeta valence quality for H to Rn: design and assessment of accuracy. *Phys Chem Chem Phys* 7(18):3297–3305
- Sagan F, Filas R, Mitoraj MP (2016) Non-covalent interactions in hydrogen storage materials LiN (CH<sub>3</sub>)<sub>2</sub>BH<sub>3</sub> and KN (CH<sub>3</sub>)<sub>2</sub>BH<sub>3</sub>. *Crystals* 6(3):28
- Gao W, Feng H, Xuan X, Chen L (2012) The assessment and application of an approach to noncovalent interactions: the energy decomposition analysis (EDA) in combination with DFT of revised dispersion correction (DFT-D3) with Slater-type orbital (STO) basis set. *J Mol Model* 18(10):4577–4589
- van der Wijst T, Fonseca Guerra C, Swart M, Bickelhaupt FM, Lippert B (2009) A ditopic ion-pair receptor based on stacked nucleobase quartets. *Angew Chem Int Ed* 48(18):3285–3287
- Guerra CF, van der Wijst T, Poater J, Swart M, Bickelhaupt FM (2010) Adenine versus guanine quartets in aqueous solution: dispersion-corrected DFT study on the differences in  $\pi$ -stacking and hydrogen-bonding behavior. *Theor Chem Accounts* 125(3–6):245–252
- Qiu NX, Xue Y, Guo Y, Sun WJ, Chu W (2012) Adsorption of methane on carbon models of coal surface studied by the density functional theory including dispersion correction (DFT-D3). *Comput Theor Chem* 992:37–47
- Goerigk L, Grimme S (2010) Efficient and accurate double-hybrid-meta-GGA density functionals—evaluation with the extended GMTKN30 database for general main group thermochemistry, kinetics, and noncovalent interactions. *J Chem Theory Comput* 7(2):291–309
- Lu T, Manzetti S (2014) Wavefunction and reactivity study of benzo [a] pyrene diol epoxide and its enantiomeric forms. *Struct Chem* 25(5):1521–1533
- Goerigk L, Grimme S (2011) A thorough benchmark of density functional methods for general main group thermochemistry, kinetics, and noncovalent interactions. *Phys Chem Chem Phys* 13(14):6670–6688

40. Neese F (2012) The ORCA program system. *Comput Mol Sci* 2(1): 73–78
41. Weigend F (2002) A fully direct RI-HF algorithm: implementation, optimised auxiliary basis sets, demonstration of accuracy and efficiency. *Phys Chem Chem Phys* 4(18):4285–4291
42. Su P, Li H (2009) Energy decomposition analysis of covalent bonds and intermolecular interactions. *J Chem Phys* 131(1):014102
43. Schmidt MW, Baldridge KK, Boatz JA, Elbert ST, Gordon MS, Jensen JH, Windus TL et al. (1993) General atomic and molecular electronic structure system. *J Comput Chem* 14(11): 1347–1363
44. Johnson ER, Keinan S, Mori-Sanchez P, Contreras-Garcia J, Cohen AJ, Yang W (2010) Revealing noncovalent interactions. *J Am Chem Soc* 132(18):6498–6506
45. Lu T, Chen F (2012) Multiwfn: a multifunctional wavefunction analyzer. *J Comput Chem* 33(5):580–592
46. Humphrey W, Dalke A, Schulten K (1996) VMD: visual molecular dynamics. *J Mol Graph* 14(1):33–38
47. Bader RF, Carroll MT, Cheeseman JR, Chang C (1987) Properties of atoms in molecules: atomic volumes. *J Am Chem Soc* 109(26): 7968–7979
48. Gadre SR, Yeole SD, Sahu N (2014) Quantum chemical investigations on molecular clusters. *Chem Rev* 114(24):12132–12173
49. Saha A, Raghavachari K (2013) Dimers of dimers (DOD): a new fragment-based method applied to large water clusters. *J Chem Theory Comput* 10(1):58–67
50. Li W, Li S, Jiang Y (2007) Generalized energy-based fragmentation approach for computing the ground-state energies and properties of large molecules. *J Phys Chem A* 111(11):2193–2199
51. Dahlke EE, Truhlar DG (2007) Electrostatically embedded many-body expansion for large systems, with applications to water clusters. *J Chem Theory Comput* 3(1):46–53
52. Yuan D, Shen X, Li W, Li S (2016) Are fragment-based quantum chemistry methods applicable to medium-sized water clusters? *Phys Chem Chem Phys*
53. Brennan JK, Bandosz TJ, Thomson KT, Gubbins KE (2001) Water in porous carbons. *Colloids Surf A Physicochem Eng Asp* 187: 539–568
54. Wu J, Wang J, Liu J, Yang Y, Cheng J, Wang Z, Zhou J, Cen K (2017) Moisture removal mechanism of low-rank coal by hydrothermal dewatering: physicochemical property analysis and DFT calculation. *Fuel* 187:242–249
55. Del Bene J, Pople JA (1969) Intermolecular energies of small water polymers. *Chem Phys Lett* 4(7):426–428
56. Salame II, Bandosz TJ (1999) Experimental study of water adsorption on activated carbons. *Langmuir* 15(2):587–593
57. Naono H, Hakuman M, Shimoda M, Nakai K, Kondo S (1996) Separation of water and ethanol by the adsorption technique: selective desorption of water from micropores of active carbon. *J Colloid Interface Sci* 182(1):230–238
58. Liu J, Wu J, Zhu J, Wang Z, Zhou J, Cen K (2016) Removal of oxygen functional groups in lignite by hydrothermal dewatering: an experimental and DFT study. *Fuel* 178:85–92
59. Brennan JK, Thomson KT, Gubbins KE (2002) Adsorption of water in activated carbons: effects of pore blocking and connectivity. *Langmuir* 18(14):5438–5447
60. Murray JS, Politzer P (1998) Electrostatic potentials: chemical applications. *Encycl Comput Chem*
61. Murray JS, Politzer P (2011) The electrostatic potential: an overview. *Comput Mol Sci* 1(2):153–163
62. Hohenstein EG, Sherrill CD (2009) Effects of heteroatoms on aromatic  $\pi-\pi$  interactions: benzene–pyridine and pyridine dimer. *J Phys Chem A* 113(5):878–886
63. Galabov B, Ilieva S, Schaefer HF (2006) An efficient computational approach for the evaluation of substituent constants. *J Org Chem* 71(17):6382–6387
64. Suresh CH, Gadre SR (2007) Electrostatic potential minimum of the aromatic ring as a measure of substituent constant. *J Phys Chem A* 111(4):710–714
65. DiLabio GA, Piva PG, Kruse P, Wolkow RA (2004) Dispersion interactions enable the self-directed growth of linear alkane nanostructures covalently bound to silicon. *J Am Chem Soc* 126(49): 16048–16050
66. Manzetti S, Lu T (2013) The geometry and electronic structure of Aristolochic acid: possible implications for a frozen resonance. *J Phys Org Chem* 26(6):473–483
67. Umeyama H, Morokuma K (1977) The origin of hydrogen bonding. An energy decomposition study. *J Am Chem Soc* 99(5):1316–1332
68. Zhechkov L, Heine T, Patchkovskii S, Seifert G, Duarte HA (2005) An efficient a posteriori treatment for dispersion interaction in density-functional-based tight binding. *J Chem Theory Comput* 1(5):841–847
69. London F (1930) Zur theorie und systematik der molekularkräfte. *Z Phys* 63(3–4):245–279
70. Dubinin MM (1980) Water vapor adsorption and the microporous structures of carbonaceous adsorbents. *Carbon* 18(5):355–364
71. Lagorsse S, Campo MC, Magalhaes FD, Mendes A (2005) Water adsorption on carbon molecular sieve membranes: experimental data and isotherm model. *Carbon* 43(13):2769–2779